A&A 382, 312–318 (2002)
DOI: 10.1051/0004-6361:20011582

Astronomy & Astrophysics

Center-to-limb-variation of the *G*-band lines at 430.5 nm

K. Langhans and W. Schmidt

Kiepenheuer–Institut für Sonnenphysik, Schöneckstr. 6, 79104 Freiburg, Germany

Received 10 September 2001 / Accepted 8 November 2001

Abstract. We measure the center-to-limb-variation of the CH lines in the wavelength range from 430.40 to 430.61 nm (*G*-band) for both quiet sun and for the cooler atmophere of sunspot umbrae at different heliographic positions. The limb effect of the CH lines is about 650 ms^{-1} at $\mu = 0.1$ with a slope similar to weak Fe lines. We investigate the behaviour of the CH abundance in the range of optical depth ($\tau = -0.05$ to $\tau = -0.25$) that is accessible by center-to-limb observations. The CH abundance decreases with height in accordance with recent numerical models.

Key words. Sun: atmosphere, photosphere

1. Introduction

The CH absorption band at 430.6 nm (*G*-band) is often used as a diagnostic tool for investigating the nature of photospheric bright points (e.g. Muller & Roudier 1984; Berger et al. 1995). Early spectroscopic observations of the *G*–band were done by Hunaerts (1947), the first center-to-limb measurements by Pecker & Peyturaux (1948) and Pecker (1949).

Most spectroscopic observations in the *G*-band are restricted to a few lines within the $^2\Delta$–$^2\Pi$ system that are listed as unblended by Moore et al. (1966). These measurements were mainly used to examine the quality of atmospheric models by comparison of observed and calculated equivalent widths of the selected CH lines. A collection of these measurements is given by Grevesse & Sauval (1973). Withbroe (1967) and Drake & Ezerinsh (1984, 1985a,b) take into account the center-to-limb-variation of the equivalent width. Withbroe (1967) estimated the height of formation for the CH lines from $\log \tau_{500} = -0.5$ to $\log \tau_{500} = -2.5$. Synthetic *G*–band spectra both for quiet sun and magnetic fluxtube models were calculated by Steiner et al. (2001) and Sánchez Almeida et al. (2001).

Many observations in the *G*–band are done in order to investigate the photospheric bright points and the connected magnetic elements, making use of the increased contrast of these structures when observed through *G*-band pass filters. There exist theoretical explanations to this effect by Kiselman et al. (2000), Rutten et al. (2001), Steiner et al. (2001) and Sánchez Almeida et al. (2001), who all calculate synthetic *G*–band spectra both for quiet sun and magnetic fluxtube models. Langhans et al. (2001) confirm the CH line weakening in bright points by direct spectroscopic observation.

Here we present the results of the center-to-limb-variation of the wavelength range 430.40 to 430.61 nm. This includes the analysis of a dataset for the quiet sun and a smaller one for sunspots with a diameter larger than 4 arcsec.

Send offprint requests to: K. Langhans,
e-mail: kai@kis.uni-freiburg.de

2. Observations and data reduction

2.1. Specification of the spectral range

The *G*-band is a molecular bandhead in the solar spectrum at around 430 nm, mainly consisting of electronic transitions between rotational and vibrational sublevels of the CH molecule. Further more it contains several atomic lines, many of them are blended with CH lines or vice versa. The high line density results in the absence of a real continuum in the whole bandhead. Figure 1 shows the observed spectral range in the *G*-band. This range was chosen because there exist "reasonably well" separated CH lines, see Table 1. At 430.41 nm the intensity almost reaches continuum level.

2.2. Observations

The data presented here were acquired in May 2000 at the Vacuum Tower Telecope (VTT), Observatorio del Teide on Tenerife, Spain. The data consist of spectra, obtained with the Echelle Spectrograph, in the *G*–band (430.40 to 430.61 nm) and in the range of 553.72 to 554.0 nm. Together with the spectra slit jaw images were taken using a 0.89 nm bandpass filter centered at 430.6 nm. The slit width was 60 μm, which corresponds to 0.3 arcsec. The data were taken with two XEDAR-cameras with 2048 × 2048 pixels, using 2 × 2 hardware binning.

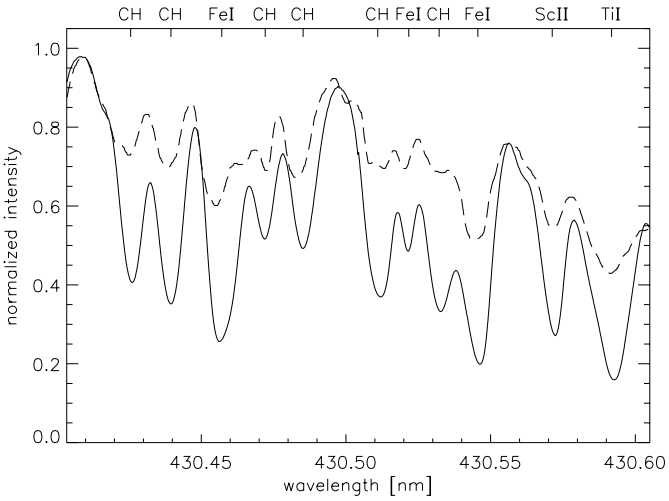

Fig. 1. The observed *G*-band spectrum (430.40 nm to 430.61 nm). The solid line represents the mean spectrum of quiet sun at disk center, the dashed line shows a mean spot spectrum. (The spot spectrum is, quite arbitrarily, scaled to the "pseudo continuum" of the quiet sun spectrum at 430.41 nm.)

Table 1. Absorption lines in the selected wavelength range of the *G*-band.

no		λ [nm]	blends
0	CH	430.4256	
1	CH	430.4395	
2	FeI	430.4571	CH
3	CH	430.4721	
4	CH	430.4852	FeI
5	CH	430.5110	FeI
6	FeI	430.5217	
7	CH	430.5322	
8	FeI	430.5456	SrII
9	ScII	430.5713	
10	TiI	430.5918	

The sampling (after binning) of the raw data was 0.135 arcsec/pixel along the slit, with a dispersion of 0.21 pm/pixel in the *G*-band and 0.27 pm/pixel around 554.0 nm.

The spectrograph slit was inclined by $-32°$ relative to the solar equator in an earth bound-coordinate system (see Fig. 2). We measured the center-to-limb-variation in slit direction [EW] and perpendicular to this axis [SN]. The slit height was 138 arcsec. For EW we scanned across the solar disk in steps of 100 arcsec to get an overlap between the single mesurements. For the SN measurements, where the slit was orientated parallel to the solar limb, the distance of the single measurements varied from 10 arcsec near the limb to 30 arcsec near disk center. In each position we took 2 exposures.

Sunspot data were taken on May 16, 17, 18, 21 and 23 at different heliographic positions to obtain the center-to-limb-variation of several *G*-band spectral lines in sunspot umbrae. The exposure times for these spectra were 12 s in the *G*-band and 2 s for the spectra around 554 nm.

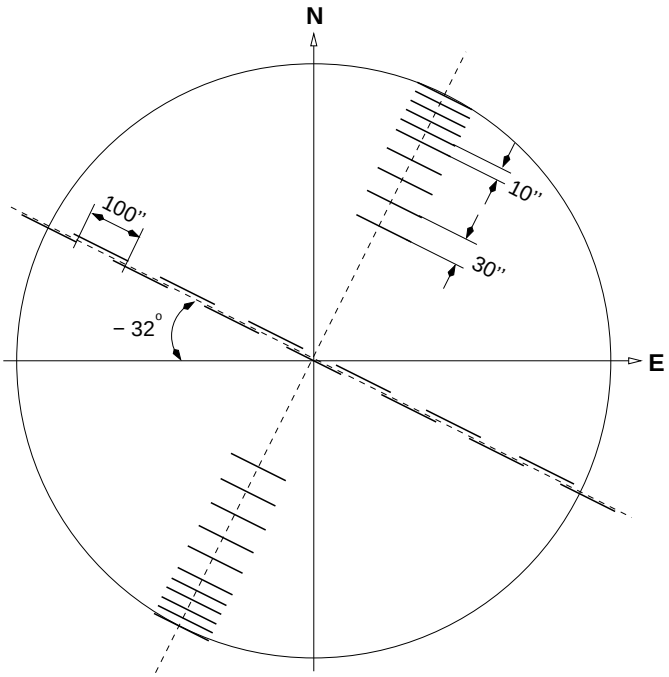

Fig. 2. Slit positions in a terrestrial coordinate system.

2.3. Data reduction

The flat field images were taken near disk center. All flat field images were subjected to dark current correction and then averaged. This average flat field image was divided spatially in five stripes and the mean line profile was calculated for each of these stripes. To obtain a gain table free of spectral information, we divided each stripe by the corresponding mean line profile.

All observed spectra were corrected for dark current and intensity offset and finally the gain table was applied in order to remove dust, CCD inhomogenities, etc. from the data. In order to improve the signal to noise ratio, the two exposures taken at the same position were added. The heliographic positions of all points along the slit were calculated. The positions given by the telescope guiding were verified and corrected if necessary. To this end, we determined the exact position of the center of the solar disk using limb-to-limb-scans in EW and SN.

To handle the data more efficiently we carried out a spatial binning in which all data points within a range of 0.5 arcsec steps were averaged. This was done separately for the EW and the SN measurements and separately for each day of observation.

Because of the absence of a clean continuum within the *G*-band, computing a scaling factor is somewhat complicated. We used the "pseudo continuum" at 430.41 nm, which, according to the Liège atlas (Delbouille et al. 1990), has an intensity of 97.78% of the "true local continuum". For the 553.72 to 554.0 nm range, there is no problem defining the continuum. Absolute continuum intensities are then taken from Neckel & Labs (1984): 4.508 (3.585) W cm^{-2} ster^{-1} nm^{-1} at 430.41 (553.88) nm. Since Delbouille et al. (1990) and Neckel & Labs (1984) used

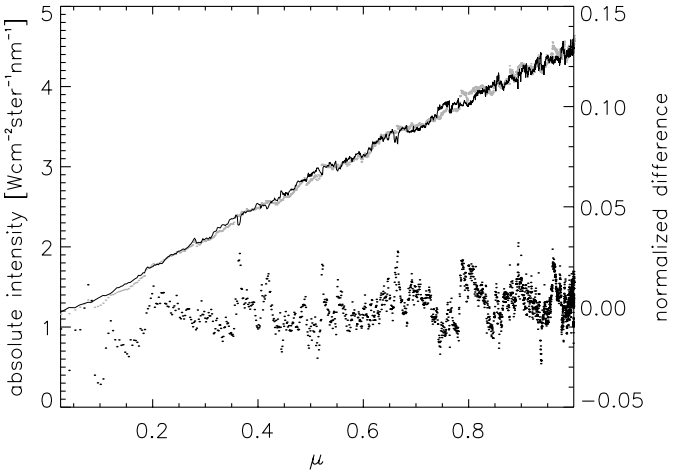

Fig. 3. The grey and the black curves represent the absolute intensity ("pseudo continuum") for the data, obtained on two different days. The dots represent the normalized difference of both intensity curves (scale at right).

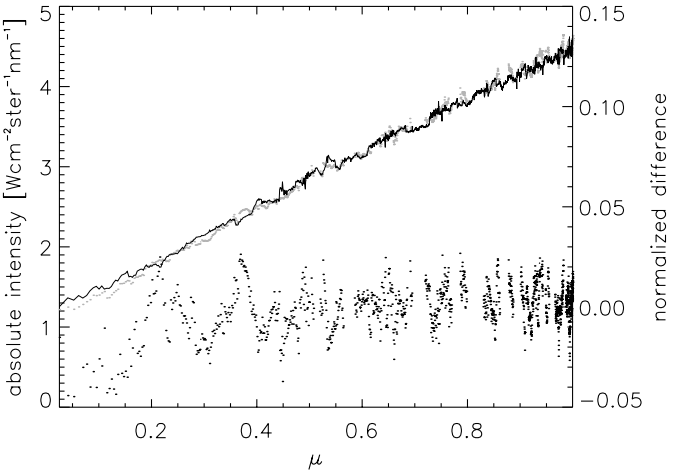

Fig. 4. The grey curve represents the absolute intensity ("pseudo continuum") for the SN data, averaged over all days of observation, as a function of the position angle $\mu\,(=\cos\vartheta)$. The black curve shows the EW data of a single scan (May 19). The dots represent the normalized difference of the SN and EW measurements (scale at right).

their own, subjective methods to define the continuum intensity in the G-band, the scaling factor is necessarily uncertain.

3. Center-to-limb variation

3.1. Error estimation

The comparison of data from two different observing days provides an estimation for the variation of the data. In Fig. 3 the intensity data ("pseudo continuum") for two days of observation (May 16, May 19) are plotted separately. The plotted absolute intensity data is an average of the EW and SN measurements. The normalized difference of the data shows that the data differ by about 1.5% (rms) over the whole range of μ. This variation could have been caused by large-scale solar structures, although no obvious candidates could be seen in the slit-jaw images, calibration errors or some unidentified instrumental problem.

3.2. EW and SN measurements

In order to estimate the potential influence of magnetic activity on the center-to-limb-variations we compared the slope of single EW measurements and the averaged SN measurements. In Fig. 4 the absolute intensities of the "pseudo continuum" are plotted. The normalized difference of the SN data curve and the EW data curve shows that there is no significant difference between the measurements, so we may use their average. (See also the comparison from data of different observing days in Fig. 3.)

3.3. Seeing effects

The error in position due to the seeing effects increases rapidly with decreasing μ. For $\mu < 0.15$ this error becomes important (note that $\mu = 0.15$ corresponds to a limb distance of only 11 arcsec). Figure 5 shows an error

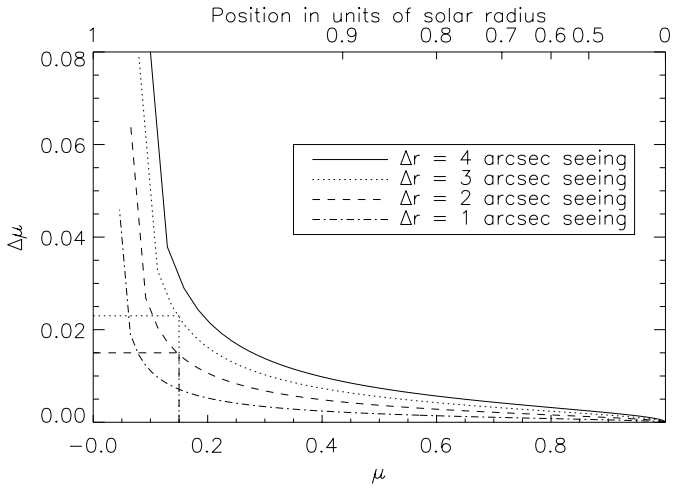

Fig. 5. The error variation estimated for different seeing conditions. The error $\Delta\mu$ is given in units of μ at the corresponding position. The plot relates the position uncertainty, Δr, to the uncertainty of the position angle, $\Delta\mu$, at position μ.

estimation for different seeing conditions. Seeing conditions of 2 arcsec (broken line) results in an uncertainty of $\Delta\mu = 0.015$ at $\mu = 0.15$, which corresponds to an error in position of 10%. 3 arcsec seeing (dotted line) results in an error of 15% in position at $\mu = 0.15$. We estimated a seeing between 2 and 3 arcsec for our observations, consequently we limited all further analysis to the range $0.15 < \mu < 1$.

3.4. Comparison to the center-to-limb-variation measurements of Neckel

Neckel (1996) describes the limb-darkening data published by Neckel & Labs (1994) by means of the functions $L_n(\mu)$. Neckel's $L_4(\mu)$ was used to describe the limb-darkening for the wavelength of 430.41 nm and 553.88 nm, shown

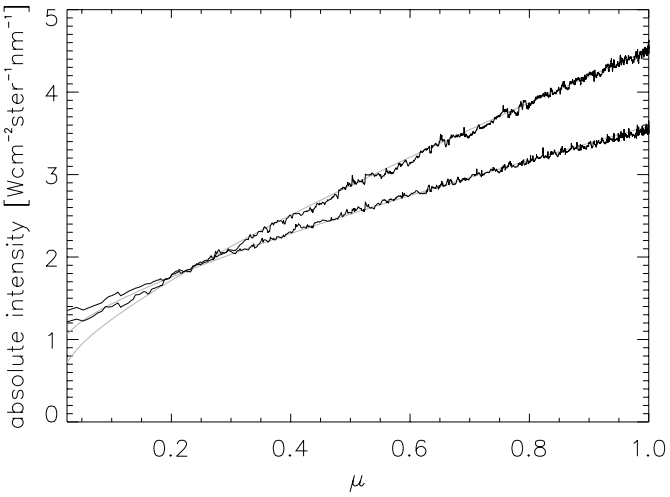

Fig. 6. The upper curves represent our G-band data (black) for the absolute intensity ("pseudo continuum") and the function $L_4(\mu)$ calculated by Neckel (1996) at 430.41 nm (grey). The lower curves represent our data for the absolute intensity (continuum) and the function $L_4(\mu)$ at 553.88 nm.

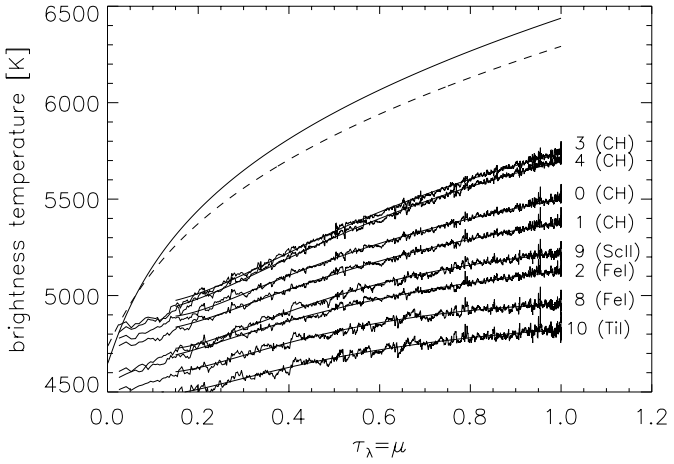

Fig. 7. Brightness temperatures. The uppermost curve corresponds to the "pseudo continuum" at 430.41 nm represented by the function $L_4(\mu)$. The broken curve corresponds to continuum at 500 nm. The other curves are based on the absolute line core intensities. Numbers refer to lines in Table 1. Thick curves correspond to our data, thin ones to the corresponding $L_4(\mu)$ functions.

in Fig. 6 (grey curves). Our averaged data is represented by the black curves. The plot shows that the data for $\mu(=\cos\vartheta) > 0.15$ fits well to the curves given by the method of Neckel.

3.5. Brightness temperatures

Brightness temperatures $T_\mathrm{b}(\mu)$ are obtained from the measured absolute intensities $I_\lambda(\mu)$ by inversion of the relation

$$I_\lambda(\mu) = B_\lambda(T_\mathrm{b}(\mu)), \tag{1}$$

where B_λ is the Planck function. According to the Eddington-Barbier relation we also have

$$I_\lambda(\mu) = S_\lambda(\tau_\lambda = \mu), \tag{2}$$

where S_λ is the source function and τ_λ the monochromatic optical depth, and assuming LTE line formation, i.e. $S_\lambda(\tau_\lambda) = B_\lambda(T(\tau_\lambda))$, we can immediately identify $T_\mathrm{b}(\mu)$ with the temperature T at $\tau_\lambda = \mu$.

Withbroe (1967) concluded that LTE is convenient to describe CH absorption. That was confirmed by calculations of Sánchez Almeida et al. (2001) and Steiner et al. (2001). A measurement of the center-to-limb-variation provides the possibility to examine T over a small height range.

Figure 7 shows the brightness temperatures as a function of monochromatic optical depth τ_λ, corresponding to μ, derived from Neckel's $L_4(\mu)$ at 430.41 nm (uppermost solid curve) and 500 nm (dasked curve) as well as for selected line cores (numbers as in Table 1) from our data.

For each line we plot the actual $T_\mathrm{b}(\mu)$ as well as the much smoother brightness temperatures derived from the $L_4(\mu)$ function fit to the intensity data.

The formation height of the line cores, more specifically the optical depth τ_lc at line center as a function of the standard optical depth τ_{500} at 500 nm, follows from the observation that we have a unique temperature at each height in the atmosphere.

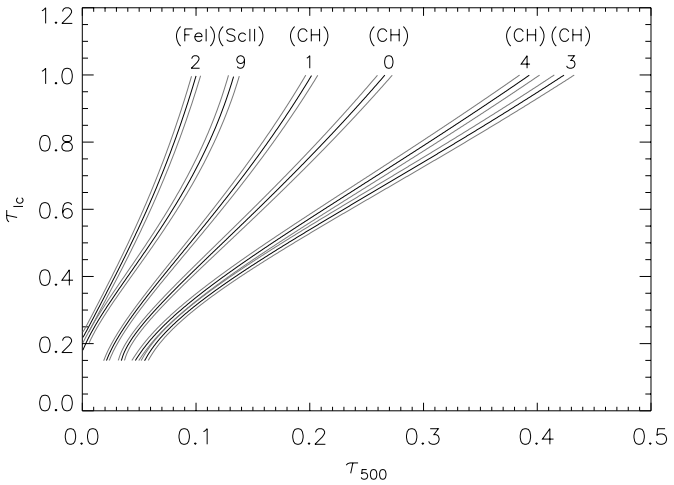

Fig. 8. τ_lc as a function of τ_{500} for selected lines (Table 1). The thin curves indicate the 1σ-level.

For each line core we can compare $T(\tau_\lambda)$ with $T(\tau_{500})$ and derive the $\tau_\lambda(\tau_{500})$ curves that are plotted in Fig. 8. The thick curves result from the $L_4(\mu)$ fits in Fig. 7, and the thin curves indicate the 1σ-level computed from the standard deviation between the fit and the data within a moving interval of $\Delta\tau = 0.1$.

3.6. CH-abundance

The optical depth, for continuum and line core repectively, can be described by the following equations

$$\mathrm{d}\tau_\mathrm{cont} = -\alpha_\mathrm{cont}\,\rho(z)\,\mathrm{d}z \tag{3}$$

$$\mathrm{d}\tau_\mathrm{lc} = -\alpha_\mathrm{lc}\,f_\mathrm{line}(z)\,\rho(z)\,\mathrm{d}z\ , \tag{4}$$

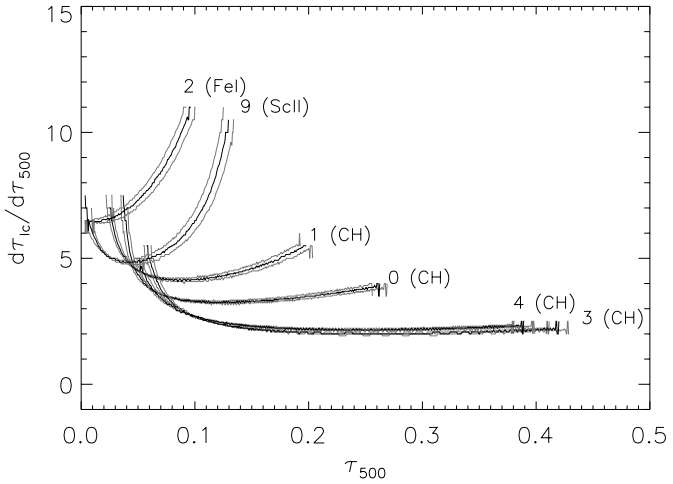

Fig. 9. The ratio $d\tau_{lc}/d\tau_{cont}$ as a function of τ_{500} for selected lines (Table 1). The thin lines indicate the 1σ-level.

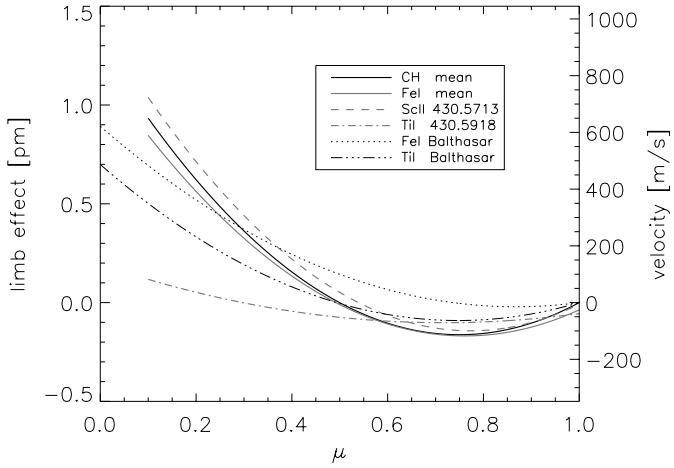

Fig. 10. The limb effect of the lines within the observed spectral range, averaged over CH and FeI lines. The results of Balthasar (Balthasar 1984b,a) are shifted to $v = 0$ at disk center.

where z is the geometrical height, $\rho(z)$ the mass density and α the absorption coefficient per unit mass. $f_{\rm line}(z)$ represents the fraction of the absorbing particles as a function of $\rho(z)$. That means that the differential quotient

$$\frac{d\tau_{\rm lc}}{d\tau_{\rm cont}} = \frac{\alpha_{\rm lc}}{\alpha_{\rm cont}} f_{\rm line}(z) \tag{5}$$

is proportional to $f_{\rm line}(z)$.

In Fig. 9 the ratio $d\tau_{lc}/d\tau_{500}$ is plotted as a function of τ_{500}. For all CH lines the ratio $d\tau_{lc}/d\tau_{cont}$ – therefore the CH abundance – decreases with increasing optical depth.

Drake & Ezerinsh (1985b) calculated the number densities of CH molecules and obtain the maximum value for an optical depth of $\tau_{500} = -0.5$. Steiner et al. (2001) calculated "the partial gas pressure (which is directly proportional to the (ionic) abundance) of CH [...] and FeI as a function of optical depth τ_{500}". For the τ_{500}-range, covered in this work, they find a decreasing abundance with τ for CH and FeI. Their maximum value is in the same range as the one given by Drake & Ezerinsh (1985b).

Our analysis confirms these results in the τ_{500}-range that is accessible by our observations.

4. Limb effect

We measured the shift of the line core position across the disk for each of the lines. The positions of the line cores were determined with a second order polynomial fit applied to 16 wavelength points around line center. For this analysis we used the EW data sets. Each single data set was corrected for solar rotation and the relative movement of sun and earth. Taking the line core positions in the mean spectra (disk center, quiet sun) as reference positions, we obtained line displacements for further calculations. After correction, east and west side data were put together and the datasets of the three days were averaged. The influence of supergranulation and other velocity fields is still present and not negligible for this kind of measurement. But because all lines are affected in the same way, differences between lines could be interpreted as differences in the limb effect.

The data were fitted in the range $0.15 < \mu < 1$ by a second order polynomial in the variable $(1 - \mu)$

$$f(\mu) = c_0 + c_1(1-\mu) + c_2(1-\mu)^2 . \tag{6}$$

Figure 10 shows the fits for all lines within the observed spectral range together with some results of limb effect measurements by Balthasar (Balthasar 1984b,a). Due to the similarity of the curves for CH respective Fe we averaged all CH lines and all Fe lines to improve the legibility of the figure. Both the scale of velocity and the line shift are relative ones, due to the absence of a laboratory or telluric absorption line for absolute wavelength calibration. The shift of the averaged CH line data is set to 0 at disk center. The results of Balthasar have also been shifted to $v = 0$ at disk center.

The CH absorption lines show almost the same limb effect as the observed FeI lines. Between $\mu = 1$ and $\mu = 0.75$ we find a decrease of the wavelength and an increase towards the limb. For the CH lines we find a limb effect of about 650 $\rm ms^{-1}$ at $\mu = 0.1$. For the observed FeI lines we find an insignificantly smaller velocity at $\mu = 0.1$, for the observed SrII line an insignificantly larger velocity. The maximal blueshift reached at $\mu = 0.75$ for FeI and CH lines is about 110 $\rm ms^{-1}$. The observed TiI line shows a lower blueshift at $\mu = 0.75$ and a limb effect below 100 $\rm ms^{-1}$ at $\mu = 0.1$.

Balthasar (Balthasar 1984a,b) averaged over a large sample of lines, but each limb effect measurement of a single line was only based on up to four independent measurements (at 13 different positions across the disk). Therefore the influence of velocity fields is not negligible. Concerning the increasing redshift toward the limb he did not find an explicit dependence on the formation height. Concerning the blueshift around $\mu = 0.8$ he found that lines formed in deeper layers show larger blueshifts than those from higher

layers, which he explained by the contribution of horizontal granular motion to the limb effect (see Balthasar 1985). Concerning the excitation energy he found that lines with low excitation energy (which is anticorrelated to the formation height) have larger redshifts. For ionized elements he found larger redshifts than for neutral ones.

In general the limb effect, measured by Balthasar (1984a,b) – using 96 Fe lines and a few other atomic lines – is smaller than the results we obtain from our observations. We find qualitative agreements; an increasing blueshift down to $\mu \cong 0.8$ and an increasing redshift when approaching the limb. The SrII line shows the largest limb effect in agreement with Balthasar's observations of ionized lines. The sample of Balthasar is dominated by lines with higher excitation energy (2.95 to 3.55 eV) which may explain the difference to the here observed iron lines. One point is remarkable following the conclusions of Balthasar: The observed limb effect for the CH lines show both a large redshift towards the limb and a blueshift relative to disk center at about $\mu = 0.8$. A large redshift towards the limb is typical for ionized elements and observed for lines with low exitation energy which includes a relative high formation, whereas a blueshift relative to disk center is not typical for ionized elements, but observed for lines with relative low formation height ($-2.5 < \tau_{500} < -1$).

5. Spots

5.1. CH line intensity in sunspot umbrae

The mean *G*–band spectrum of an umbra (Fig. 1) shows that the CH lines still exist, but they are more weakened than the atomic lines. The plotted umbra spectrum is averaged over the two largest spots during the days of observations (leading spots of AR 9002 and 8996). In the range between 430.49 and 430.60 nm, where the line centers are isolated and not blended, the CH line weakening in comparison to the Fe line weakening is obvious. The relative line depth of the FeI line at 430.5217 nm is 22% less than in the mean quiet sun spectrum whereas the CH lines has decreased by 35% on average. Figure 11 shows the intensity curve along the spectrograph slit of the leading spot of group 8996 (May 17) for the pseudo continuum at 430.41 nm and for a CH line core. The intensity outside the spot is normalized to unity for both wavelengths. The contrast I_U/I_{QS} differs by a factor of two between the continuum and the CH line core.

5.2. Center-to-limb-variation of Sunspot data

In each spectrum of sunspots we averaged over the inner part of the umbra, over a part of the penumbra and – if available in the same spectrum – over a range of the quiet sun. For all these spectra we estimated the absolute intensities for line cores and the "pseudo continuum". Assuming LTE we convert the absolute intensities again to brightness temperatures.

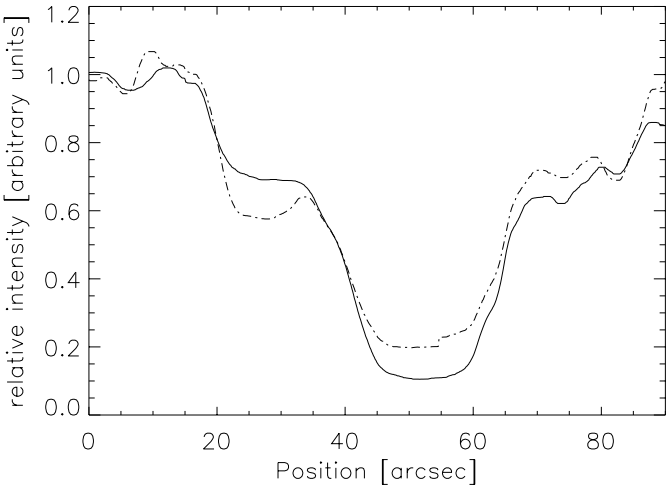

Fig. 11. Intensity across a sunspot (AR 8996, May 17), measured along the spectrograph slit. The solid curve represents the spot section seen in "pseudo continuum" at 430.41 nm, the broken curve corresponds to a CH line core.

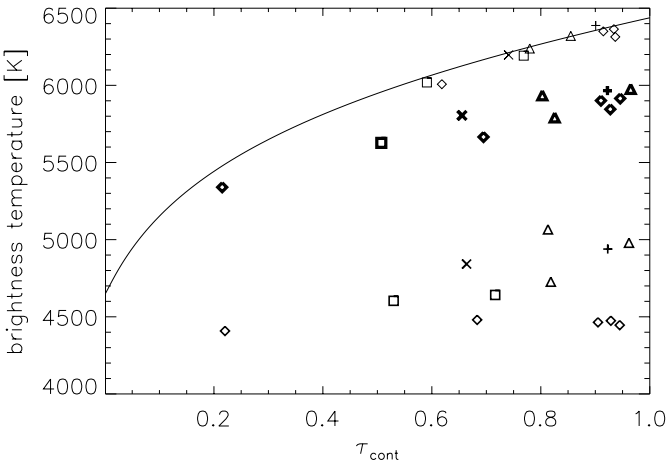

Fig. 12. Brightness temperatures of the "pseudo continuum" for the quiet sun (thin symbols), penumbra (thick) and umbra (medium). Same symbols mark the same sunspot during the days of observation.

In Fig. 12 the brightness temperature of the "pseudo continuum" is plotted for quiet sun (thin symbols), penumbra (thick) and umbra (medium) for all positions measured during the days of observation. The data points that belong to the same sunspot on different days are marked by same symbols. The points of quiet sun measurements agree well with the curve of Labs and Neckel for 430.41 nm.

The brightness temperatures of the different sunspots vary in a range of 500 K, but the center-to-limb-variation of a single sunspot covers only a small temperature range. The line core intensities in the umbra do not show a difference either. The leading spot of AR 8996 (in Fig. 12 represented by ◇) does not show a center-to-limb-variation in the umbra.

Similar to the line core intensities of our center-to-limb quiet sun data (see Sect. 3.5) we fitted the penumbra

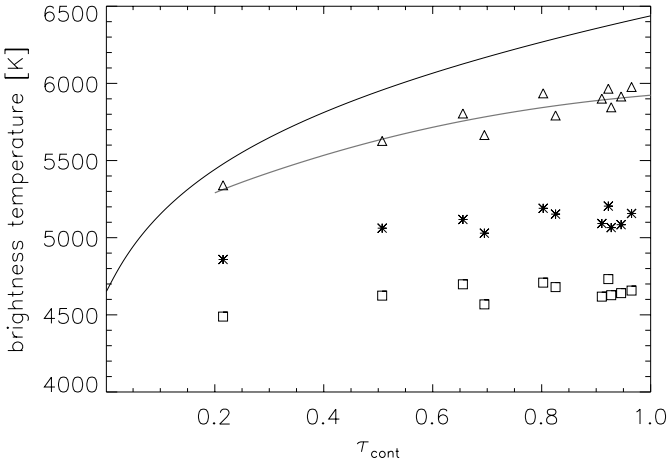

Fig. 13. Brightness temperatures. The uppermost solid curve corresponds to the "pseudo continuum" in the quiet sun based on the function $L_4(\mu)$ estimated by Neckel (1996) at 430.41 nm. The other curves and symbols present temperatures for the penumbra: "pseudo continuum" ($\triangle$) and fit based on a $L_4(\mu)$ function, line core temperatures for CH at 430.4395 nm ($*$) and Fe at 430.5456 nm ($\square$).

"pseudo continuum" data by a function $L_4(\mu)$ and converted that to brightness temperatures (Fig. 13). The plot also shows the line core intensities for CH at 430.4395 nm ($*$) and Fe at 430.5456 nm ($\square$).

Within the $\tau_{\rm cont}$-range ($0.2 < \tau_{\rm cont} < 1$) of our data the center-to-limb-variation of the penumbra "pseudo continuum" covers a temperature range of about 600 K while the center-to-limb-variation of the quiet sun "pseudo continuum" covers a temperature range of about 1000 K in the same $\tau_{\rm cont}$-range. The brightness temperatures for the line core data of CH and FeI do not show a significant difference in the center-to-limb-variation. As is apparent in the plot there is no overlap between the temperature range covered by the "pseudo continuum" data and the temperature range covered by the line core data. Consequently further analysis – like in Sect. 3.6 for the quiet sun – is not possible for penumbra data.

6. Discussion

Our observations support the "typical" assumptions about the *G*-band.

The center-to-limb-variation of the absolute intensities of the "pseudo continuum" and all line cores within the observed wavelength range can be described by the functions $L_4(\mu)$ (see Neckel 1996).

We find a decrease of the abundance of CH in the range of optical depth τ covered by the center-to-limb analysis ($0.15 < \tau < 1$). This is in agreement with numerical calculations of Drake & Ezerinsh (1985b), Sánchez Almeida et al. (2001) and Steiner et al. (2001), who all assumed LTE.

The strong blueshift of the CH lines at $\mu = 0.75$ – visible in the limb effect data – also indicates that these lines are formed in deep layers of the photosphere. On the other hand, the CH lines also show a strong redshift towards the limb, which, according to Balthasar (1984b, 1985, points towards line formation at greater heights. So the CH lines might form over a relatively large height range.

To confirm this conjecture further comparisons of the CH-lines with atomic lines covering a range of height within the photosphere are needed. Also it will be useful to compare these results with theoretical and numerical radiation transfer calculations.

Acknowledgements. J. Bruls and O. Steiner provided very useful hints and comments. R. Schlichenmaier helped with the observations at the VTT. One of us (K.L.) is supported by the Deutsche Forschungsgemeinschaft.

References

Balthasar, H. 1984a, Ph.D. Thesis, Universität Göttingen
Balthasar, H. 1984b, Sol. Phys., 93, 219
Balthasar, H. 1985, Sol. Phys., 99, 31
Berger, T. E., Schrijver, C. J., Shine, R. A., et al. 1995, ApJ, 454, 531
Delbouille, L., Roland, G., & Neven, L. 1990, Atlas photometrique DU spectre solaire de λ 3000 Å a λ 10000 Å (Liège: Université de Liège, Institut d'Astrophysique, 1990)
Drake, N. A., & Ezerinsh, N. V. 1984, Solnechnye Dannye. Byul. Glav. Astr. Obs., 3, 90
Drake, N. A., & Ezerinsh, N. V. 1985a, Solnechnye Dannye. Byul. Glav. Astr. Obs., 11, 72
Drake, N. A., & Ezerinsh, N. V. 1985b, Solnechnye Dannye. Byul. Glav. Astr. Obs., 9, 48
Grevesse, N., & Sauval, A. J. 1973, A&A, 27, 29
Hunaerts, J. 1947, Ann. Astrophys., 10, 237
Kiselman, D., Rutten, R. J., & Plez, B. 2000, IAU Symp., 203, E112
Langhans, K., Schmidt, W., Rimmele, T., & Sigwarth, M. 2001, in ASP Conf. Ser. 236: Advanced Solar Polarimetry – Theory, Observation, and Instrumentation, 439
Moore, C. E., Minnaert, M. G. J., & Houtgast, J. 1966, The solar spectrum 2935 Å to 8770 Å (National Bureau of Standards Monograph, Washington: US Government Printing Office (USGPO), 1966)
Muller, R., & Roudier, T. 1984, Sol. Phys., 94, 33
Neckel, H. 1996, Sol. Phys., 167, 9
Neckel, H., & Labs, D. 1984, Sol. Phys., 90, 205
Neckel, H. 1994, Sol. Phys., 153, 91
Pecker, J. 1949, Ann. Astrophys., 12, 9
Pecker, J., & Peyturaux, R. 1948, Ann. Astrophys., 11, 90
Rutten, R. J., Kiselman, D., van der Voort, L. R., & Plez, B. 2001, in ASP Conf. Ser. 236: Advanced Solar Polarimetry – Theory, Observation, and Instrumentation, 445
Sánchez Almeida, J. S., Ramos, A. A., Trujillo Bueno, J., & Cernicharo, J. 2001, ApJ, 555, 978
Steiner, O., Hauschildt, P. H., & Bruls, J. 2001, A&A, 372, L13
Withbroe, G. L. 1967, ApJ, 147, 1117